Letter

Coexistence of spectrally stable and unstable modes in black hole ringdowns

Peng Wang [1,*] and Tianshu Wu [2,1,†]

[1]*College of Physics, Sichuan University, Chengdu 610065, China*

[2]*Department of Astronomy, Tsinghua University, Beijing 100084, China*

(Received 9 March 2026; accepted 30 April 2026; published 8 July 2026)

Recent studies have shown that a secondary potential barrier, forming a potential well outside the event horizon, can destabilize the quasinormal mode (QNM) spectrum of black holes. We find that spectral instability may persist even after the potential well vanishes, giving rise to a distinct family of spectrally unstable QNMs that differ from the spectrally stable modes localized near the potential peak and associated with the photon sphere. Nevertheless, time-domain simulations reveal that early-time ringdown waveforms remain dominated by stable modes, while unstable modes have only a subdominant contribution. These results highlight the robustness of black hole spectroscopy, as the observable ringdown signal is primarily governed by the most stable QNMs.

DOI: 10.1103/srxw-wsvq

Introduction. The direct detections of gravitational waves by the LIGO-Virgo-KAGRA Collaboration have opened a new era of black hole (BH) physics [1–5], allowing us to probe the nature of strong gravity through BH spectroscopy, which measures the characteristic quasinormal modes (QNMs) emitted by a perturbed remnant BH [6–18]. Each QNM encodes information about the mass, spin, and possible deviations from the Kerr solution, providing a powerful test of general relativity in the nonlinear regime [19–32]. The success of the BH spectroscopy program crucially relies on the assumption that the QNM spectrum is physically robust and stable under small perturbations to the underlying spacetime.

Recent investigations, however, have revealed intriguing signs that this assumption may not always hold. Several studies have shown that when a small "bump" is introduced into the curvature potential governing BH perturbations, the resulting QNM spectrum can undergo drastic rearrangements or migrations, signaling spectral instability [33–43]. Complementary analyses based on the pseudospectrum have further demonstrated that the QNM operator is highly non-normal, so that even tiny perturbations in the potential can induce large spectral shifts [44–56]. These developments have raised important questions about the mathematical stability and physical interpretability of QNMs, which form the theoretical foundation of BH spectroscopy.

To assess the significance of this issue, it is essential to examine not only the frequency-domain spectrum but also the time-domain response of the system. Indeed, time-domain studies have provided reassuring evidence that the ringdown waveforms themselves remain stably perturbed even in cases where the QNM spectrum appears unstable [46,57–60]. Moreover, alternative frequency-based characterizations of BH perturbations, such as graybody factors and ringdown filters, have been shown to remain robust against the same types of perturbations that trigger spectral instability in the QNM spectrum [61–70]. These findings suggest that spectral instability may primarily reflect the mathematical sensitivity of the QNM eigenvalue problem rather than a physical instability in the observable ringdown signal.

Despite these insights, the physical mechanism underlying spectral instability remains to be clarified. From a physical perspective, spectral instability often arises in systems where the effective potential develops a potential well induced by the added bump. The appearance of this well can give rise to a new family of long-lived modes that may eventually overtake the fundamental QNM, leading to apparent spectral instability. One might thus expect that when the potential well disappears, the QNM spectrum should recover its spectral stability. However, as we will show, the situation is more subtle: even when the potential well vanishes, a residual scale inherited from the potential well can still produce a family of spectrally unstable QNMs.

This observation naturally raises a deeper question: if both spectrally stable and unstable QNM families coexist within the same system, does the presence of spectrally unstable modes necessarily lead to observable instabilities in the time-domain ringdown signal, thereby threatening the reliability of BH spectroscopy? In this Letter, we explore this question in a toy yet physically viable model: a test scalar field propagating on a static, spherically symmetric BH background in the Einstein-Maxwell-scalar (EMS) model [71–74]. By combining frequency- and time-domain analyses, we demonstrate how spectral (in)stability manifests in such systems and assess its physical impact on ringdown signals.

[*]Contact author: pengw@scu.edu.cn

[†]Contact author: wuts25@mails.tsinghua.edu.cn

Setup. In this Letter, we exam the QNM spectrum of a test scalar field in the static, spherically symmetric BH background in an EMS model. The EMS model describes a scalar field ϕ minimally coupled to the metric field and nonminimally coupled to electromagnetic field A_μ, with the action

$$S = \int d^4x\sqrt{-g}\left[R - 2(\partial\phi)^2 - e^{\alpha\phi^2}F^{\mu\nu}F_{\mu\nu}\right]. \quad (1)$$

Here, $F_{\mu\nu} = \partial_\mu A_\nu - \partial_\nu A_\mu$ is the electromagnetic field strength tensor, and $e^{\alpha\phi^2}$ is the coupling function between ϕ and A_μ. Interestingly, adopting the spherically symmetric and asymptotically flat BH ansatz

$$ds^2 = g^{\mu\nu}dx_\mu dx_\nu = -N(r)e^{-2\delta(r)}dt^2 + \frac{dr^2}{N(r)} + r^2 d\Omega, \quad (2)$$

hairy BH solutions with a nontrivial scalar field profile can be numerically constructed via the shooting or spectrum methods [71,75]. We briefly discuss in Supplemental Material [76] how to compute BH solutions using the spectral method.

For simplicity, we consider the perturbation of a massless neutral scalar field Ψ in the hairy BH background, which is governed by

$$\Box\Psi = \frac{1}{\sqrt{-g}}\partial_\mu(g^{\mu\nu}\sqrt{-g}\partial_\nu\Psi) = 0. \quad (3)$$

By decomposing the perturbation into spherical harmonics $Y_{lm}(\theta,\varphi)$, the field can be expressed as $\Psi = r^{-1}\sum_{l,m}\psi(t,r)Y_{lm}(\theta,\varphi)$. Equation (3) then reduces to the Regge-Wheeler-Zerilli-type wave equation,

$$\left(-\frac{\partial^2}{\partial t^2} + \frac{\partial^2}{\partial x^2} - V_{\mathrm{eff}}(x)\right)\psi(t,x) = 0, \quad (4)$$

where the tortoise coordinate x is determined by $dx/dr \equiv e^{\delta(r)}N^{-1}(r)$, and the effective potential is given by

$$V_{\mathrm{eff}}(x) = \frac{e^{-2\delta}N}{r^2}\left[l(l+1) + 1 - N - \frac{Q^2}{r^2 e^{\alpha\phi^2}}\right], \quad (5)$$

with Q being BH charge Q. To analyze the QNM spectrum, one typical preforms a Fourier transform $\psi(t,x) = \int d\omega\tilde{\psi}(\omega,x)e^{-i\omega t}$ that reduces the wave equation to a master equation for QNMs,

$$\left(\frac{d^2}{dx^2} + \omega^2 - V_{\mathrm{eff}}(x)\right)\tilde{\psi}(\omega,x) = 0. \quad (6)$$

Subsequently, QNMs are determined by imposing purely ingoing waves at the horizon and purely outgoing waves at infinity, yielding a discrete set of QNMs with complex frequencies $\omega_n = \omega_R + i\omega_I$, where $n = 0,1,2\ldots$ denotes the overtone number.

Nevertheless, computing QNMs—especially overtones—of BHs is numerically challenging when the background BH solution is constructed numerically. To minimize numerical errors, we employ spectral methods with identical resolutions to compute both the background BH solution and its associated QNMs. The metric functions are evaluated directly at the spectral grid points, and these values are subsequently used to construct the coefficients of the QNM master equation (6) on the same grid, thereby ensuring consistency and reducing interpolation errors. Alternatively, one can evolve the wave equation (4) in time and extract QNMs from the resulting waveform. All technical details of our numerical implementation, additional calculations, and supplementary physical discussions are presented in Supplemental Material [76] (see also Refs. [77–84] therein).

QNM spectrum. For hairy BH backgrounds with $\alpha = 0.8$ and varying charge-to-mass ratio Q/M, we compute the QNMs of the scalar field Ψ for $l = 2$ and $l = 10$, as shown in Figs. 1 and 2, respectively. The left panels display the trajectories of the first few QNM frequencies in the complex plane as Q/M varies, illustrating how the QNM spectrum migrates with respect to Q/M. The upper-right panels show the square of the real part of the QNM frequency, ω_R^2, as a function of Q/M, together with the effective potential V_{eff} for several representative values of Q/M. The relative position of ω_R^2 with respect to V_{eff} provides insights into the physical origin of the QNMs. For instance, modes with ω_R^2 near a potential peak or within a potential valley correspond, respectively, to oscillations around the photon sphere and to quasibound states trapped inside the valley [85–88].

Interestingly, unlike Schwarzschild or Reissner-Nordström BHs, the effective potential V_{eff} of hairy BHs can develop a double-peaked structure when Q/M is sufficiently large. The portion of the frequency trajectories lying beyond (upper right of) blue triangles in the left panels, along with the QNMs in the cyan-shaded regions of the right panels, correspond to this double-peaked regime. Moreover, the upper-right panels reveal that V_{eff} transitions from a double-peaked to a single-peaked profile as Q/M decreases.

We first examine the QNM spectrum of the scalar field with $l = 10$, as shown in Fig. 1. Tracing the QNM frequency trajectories from the upper-right corner, we observe that the spectrum bifurcates into two distinct families once the effective potential V_{eff} becomes single peaked. By analyzing the behavior of ω_R^2, these two families can be identified as follows:

(i) Peak modes: These modes are localized near the potential peak and are associated with the photon sphere situated near that peak. In the eikonal limit, the real part of the QNM frequency approximately equals $\sqrt{V_{\mathrm{eff}}}$ at the peak, which also determines the angular velocity of photons on the unstable circular orbit at the photon sphere [85]. The modes are

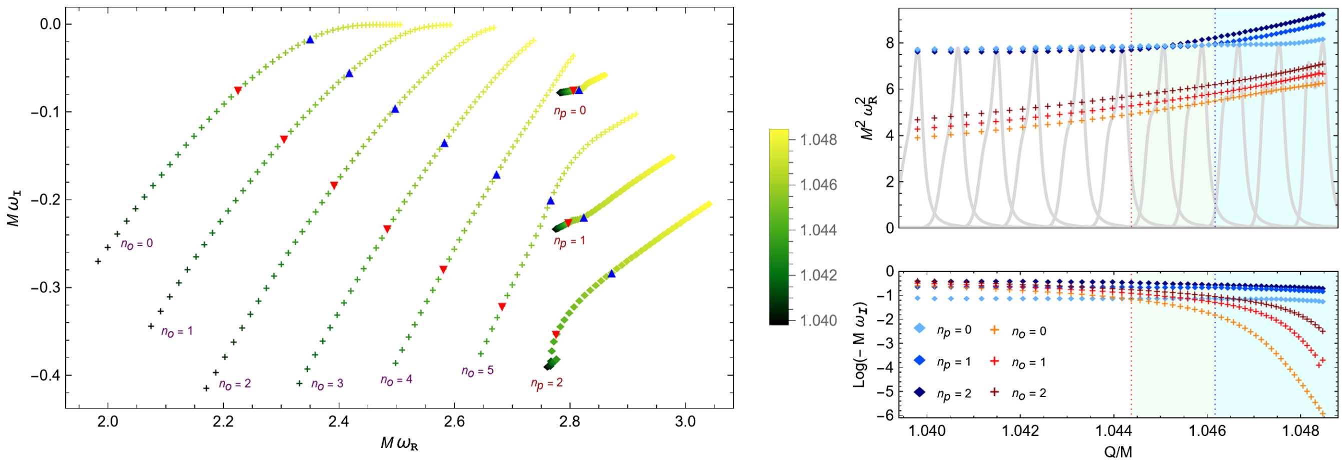

FIG. 1. QNM spectrum of the scalar field with $l = 10$ for hairy BHs with varying charge-to-mass ratio Q/M. Diamonds and plus signs denote the peak and off-peak mode families, respectively. Left: QNM trajectories in the complex-frequency plane, with the color bar indicating Q/M. Blue triangles mark the transition between the single-peaked and double-peaked regimes of $V_{\rm eff}$; the portions below and to the left of these triangles correspond to the single-peaked regime, where the off-peak modes show much larger spectral migration. Upper right: ω_R^2 as a function of Q/M, together with representative profiles of $V_{\rm eff}$. The cyan-shaded region denotes the double-peaked regime. Lower right: Imaginary parts of the QNM frequencies. The white and green regions indicate where the fundamental QNM belongs to the peak and off-peak families, respectively, and red triangles mark the overtaking event.

indexed by n_p according to their decay rates, starting from the most slowly decaying mode ($n_p = 0$). This family resembles the QNMs found in Schwarzschild and Kerr BHs and is represented by diamonds in Fig. 1.

(ii) Off-peak modes: These modes are found at an appreciable distance from the potential peak and are marked by plus signs in Fig. 1. Unlike the peak modes, they cannot be attributed to photon spheres. Remarkably, as Q/M increases and $V_{\rm eff}$ develops a double-peaked structure, the low-lying modes evolve into long-lived modes trapped within the potential valley between the two peaks. This behavior suggests that the off-peak modes in the single-peaked regime retain a residual imprint of the valley configuration present in the double-peaked regime. Similar diffraction-trapped states near the single-/double-peaked transition were recently found in a hairy Schwarzschild background [89]. The index n_o is used to label these modes in order of their decay rates, from the slowest ($n_o = 0$) to the fastest decaying.

Remarkably, in the single-peaked regime, the off-peak modes are noticeably more sensitive to variations in Q/M than the peak modes, as indicated by their larger frequency migration distances in the complex plane. This observation is further supported by the upper-right and lower-right panels of Fig. 1, which show that both the real and imaginary parts of the peak-mode frequencies exhibit much weaker spectral shifts compared to the pronounced changes of the off-peak modes. Moreover, the migration rate $\delta\omega$, defined in Supplemental Material [76], confirms that $\delta\omega$ of the off-peak modes is significantly higher than that of the peak modes. It is also noteworthy that, near and within the double-peaked regime, the fundamental peak mode ($n_p = 0$) remains spectrally stable, whereas its overtones become increasingly unstable.

Furthermore, as Q/M increases, the imaginary part of the off-peak modes decreases at a rate substantially faster than that of the peak modes. This contrasting behavior results in a level crossing, during which the fundamental QNM—initially identified as the $n_p = 0$ peak mode—is overtaken by the $n_o = 0$ off-peak mode. The QNMs at the point of this overtaking are indicated by red triangles in the complex frequency plane. Notably, this transition is accompanied by a clear discontinuity in the real part of the fundamental QNM frequency and by the onset of destabilization of the fundamental mode itself.

Figure 2 illustrates the spectral migration of the QNM spectrum as Q/M varies for the $l = 2$ case. Similar to the $l = 10$ case discussed earlier, the spectrum in the single-peaked regime consists of two distinct families: the peak modes and the off-peak modes, between which a fundamental QNM overtaking occurs. However, a notable difference arises for $l = 2$: the residual influence of the potential valley, a remnant of the double-peaked structure, exerts a much stronger effect on the QNMs in the single-peaked regime. This enhanced influence renders the $n_p = 2$ overtone of the peak-mode family spectrally unstable, resembling the behavior of the off-peak modes. In contrast, the $n_p = 0$ and $n_p = 1$ peak modes remain spectrally stable, provided that Q/M stays sufficiently far from the range associated with the double-peaked $V_{\rm eff}$. Moreover, in the double-peaked regime, the potential valley is considerably shallower in the $l = 2$ case, so that only a single off-peak mode, $n_o = 0$, forms a quasibound state trapped within the valley.

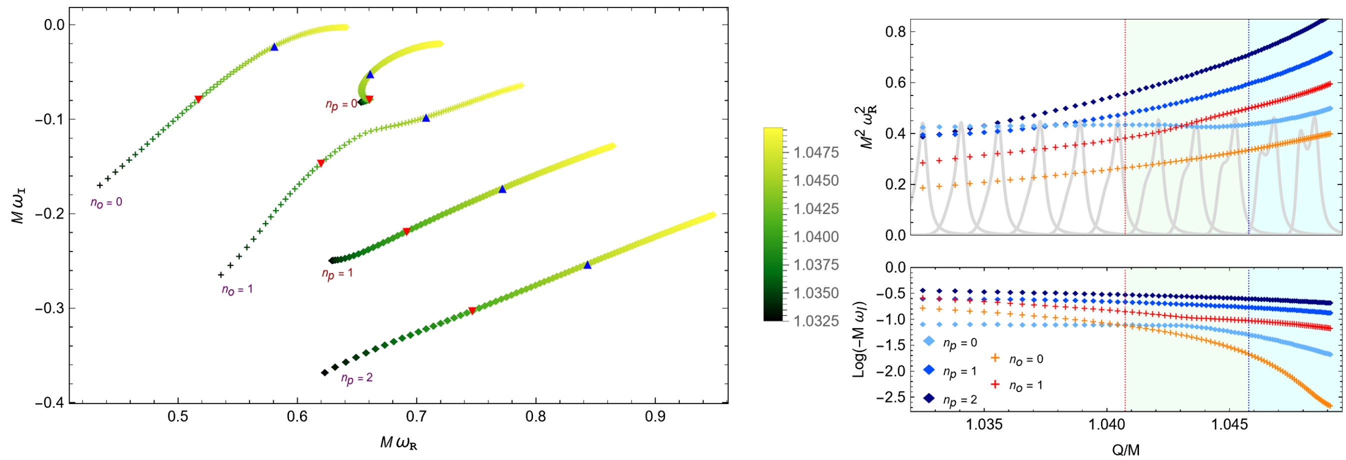

FIG. 2. QNM spectrum of the scalar field with $l = 2$ for hairy BHs. Compared with the $l = 10$ case, the remnant of the double-peaked structure has a stronger effect in the single-peaked regime, making the $n_p = 2$ peak-mode overtone spectrally unstable while leaving the $n_p = 0$ and $n_p = 1$ modes stable away from the double-peaked regime.

QNM extraction. We now examine how spectral (in)stability affects time-domain QNM extraction. We focus on two representative cases: $Q/M = 1.04436$ with $l = 10$, where the peak modes are much more spectrally stable and a fundamental-mode overtaking occurs, and $Q/M = 1.03507$ with $l = 2$, where the stability gap between the two families is smaller.

To obtain the scalar field waveforms, we numerically solve the wave equation (4) in the time domain, using a Gaussian pulse located near the potential peak as the initial data. The numerical integration procedure and the resulting waveforms are presented in Supplemental Material [76]. At late times, the waveform decays as a linear combination of exponentially damped sinusoids, whose frequencies and damping rates can be extracted by fitting the signal with an N-mode template,

$$\psi(t) = \mathrm{Re}\sum_{n=0}^{N-1} A_n e^{-i(\omega_n t - \phi_n)}, \tag{7}$$

where A_n and ϕ_n denote the amplitude and phase of the nth mode, respectively.

We employ two fitting schemes for QNM extraction: (i) Strong (agnostic) fit model: All parameters $\{A_n, \phi_n, \omega_n\}$ are treated as free, and we use the NonlinearModelFit function in *Mathematica* to determine them. The extracted QNM frequencies can serve as an independent cross-check of the frequency-domain results. (ii) Weak fit model: The frequencies are fixed, and the notation (N_p, N_o) specifies the number of modes selected from the peak and off-peak families, respectively. Only $\{A_n, \phi_n\}$ are treated as fitting parameters, and the fitting is performed using the LinearModelFit function in *Mathematica*. The resulting amplitudes quantify the relative contributions of each QNM to the time-domain signal. Both fitting models are applied over the time window $[t_0, t_{\mathrm{peak}} + 300M]$, where the start time t_0 varies within $[t_{\mathrm{peak}}, t_{\mathrm{peak}} + 300M]$, and t_{peak} denotes the time corresponding to the waveform's maximum amplitude. If the waveform accurately follows the QNM model, a stable plateau region emerges in which the fitted parameters remain nearly constant across a range of start times [31,90]. More details regarding the weak fit model are provided in Supplemental Material [76].

Figure 3 presents the fitting results for the case $Q/M = 1.04436$ with $l = 10$, where the waveform is analyzed using the strong fit model with three QNMs and the weak fit model with $(N_p, N_o) = (3, 1)$. The left panel shows the QNM frequencies extracted from the strong fit model in the complex plane, with dots of varying shades representing results obtained at different start times. For reference, diamonds and plus signs indicate the frequency-domain QNMs belonging to the peak and off-peak families, respectively. Within $13 \lesssim (t_0 - t_{\mathrm{peak}})/M \lesssim 26$, the first three peak modes are successfully extracted, and their frequencies exhibit good agreement with the frequency-domain results. Furthermore, as shown in the upper-right panel, the extracted amplitudes display a clear plateau as functions of t_0, providing additional confirmation of the robustness of the fitting.

However, the strong fit model fails to extract the off-peak modes from the waveform, indicating that the peak modes dominate the QNM contribution to the time-domain signal. To assess the influence of the off-peak modes, we apply the weak fit model using the $n_0 = 0$ off-peak mode together with the first three peak modes. The extracted amplitudes are displayed in the lower-right panel, where an amplitude plateau for all four modes appears within the range $12 \lesssim (t_0 - t_{\mathrm{peak}})/M \lesssim 16$. Notably, the amplitude of the $n_0 = 0$ off-peak mode is approximately $\mathcal{O}(10^{-4})$ smaller than those of the peak modes, further confirming that the off-peak modes make a negligible contribution to the time-domain signal.

Figure 4 presents the fitting results for the case $l = 2$ with $Q/M = 1.03507$, where the waveform is analyzed

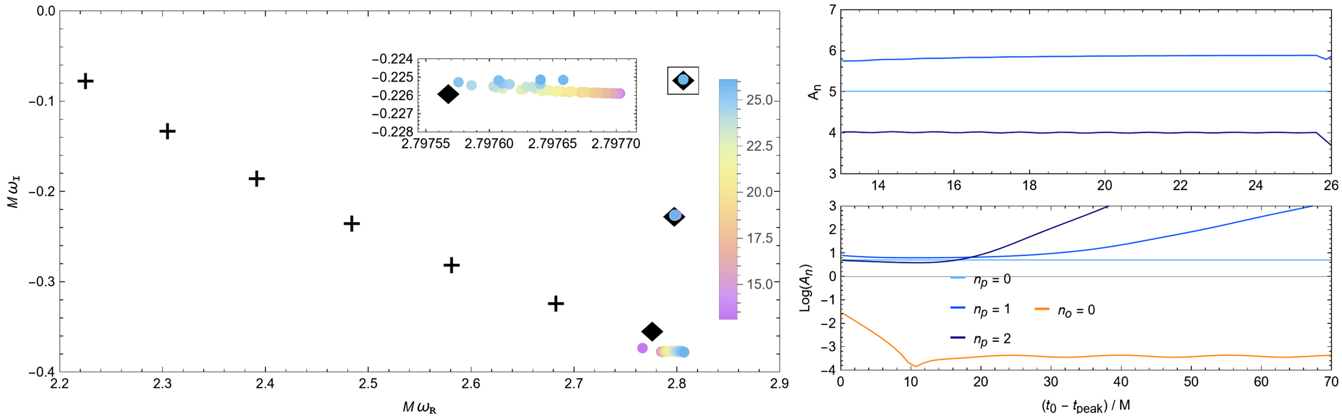

FIG. 3. QNM fitting results for $Q/M = 1.04436$ with $l = 10$. Left: Frequencies extracted from the three-mode strong fit as the start time is varied. The color bar indicates the start time. Diamonds and plus signs denote the frequencies of the peak and off-peak families computed in the frequency domain, respectively. Only the peak modes are reliably recovered. Upper right: Corresponding strong-fit amplitudes. Lower right: Weak-fit amplitudes for $(N_p, N_o) = (3, 1)$, showing that the off-peak contribution is suppressed by $\mathcal{O}(10^{-4})$ relative to the peak modes.

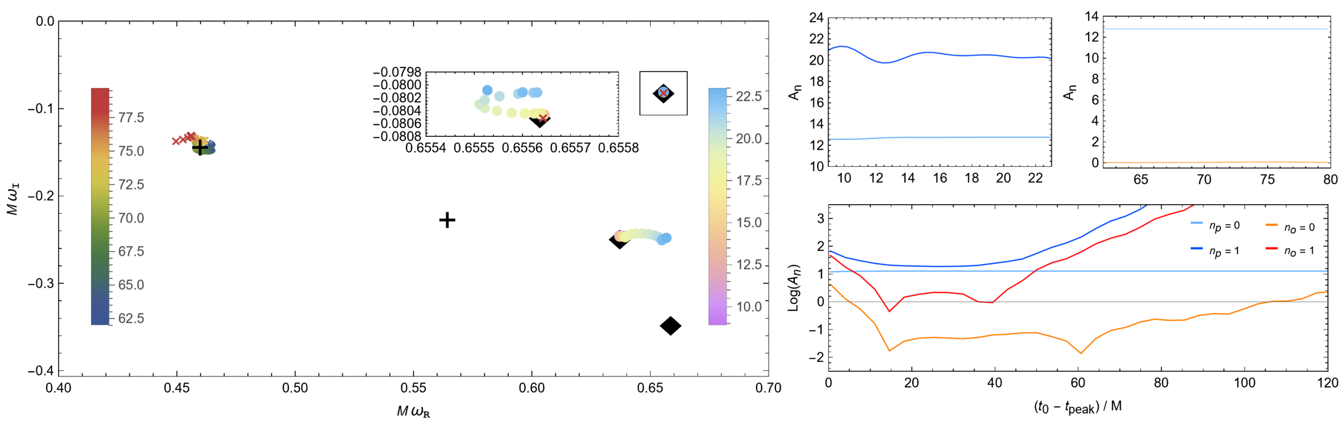

FIG. 4. QNM fitting results for $Q/M = 1.03507$ and $l = 2$. Left: Frequencies extracted from the two-mode strong fit. Dots and crosses denote early and late fitting windows, respectively. The early signal recovers only peak modes, while the late signal also recovers the $n_o = 0$ off-peak mode. Upper right: Corresponding strong-fit amplitudes. Lower right: Weak-fit amplitudes for $(N_p, N_o) = (2, 2)$, showing that the off-peak contributions are suppressed by $\mathcal{O}(10^{-3})$–$\mathcal{O}(10^{-1})$ relative to the peak modes.

using the strong fit model with two QNMs and the weak fit model with $(N_p, N_o) = (2, 2)$. The left panel shows the QNM frequencies extracted from the strong fit model in the complex plane, with dots and crosses representing results obtained from early-time windows $9 \lesssim (t - t_{\mathrm{peak}})/M \lesssim 23$ and late-time windows $60 \lesssim (t - t_{\mathrm{peak}})/M \lesssim 80$, respectively. For early-time windows, only the peak modes are successfully extracted, indicating that the early portion of the waveform is dominated by these modes. Using the weak fit model with the first two peak and off-peak modes, we find that the extracted amplitudes exhibit a clear plateau around $(t - t_{\mathrm{peak}})/M \sim 25$, as shown in the lower-right panel. The amplitudes of the $n_0 = 0$ and $n_0 = 1$ off-peak modes are approximately $\mathcal{O}(10^{-3})$ and $\mathcal{O}(10^{-1})$ smaller than those of the peak modes, respectively. For late-time windows, the strong fit model captures both the $n_p = 0$ peak mode and the $n_o = 0$ off-peak mode, which are the two slowest-decaying QNMs and thus dominate the late-time waveform. The upper-right panels further show that the $n_p = 0$ peak mode provides the most significant contribution to the late-time signal.

Conclusions. In this Letter, we studied the QNM spectrum of a test scalar field on hairy BH backgrounds using both frequency- and time-domain methods. As Q/M increases, the effective potential changes from a single-peaked to a double-peaked profile. The secondary barrier introduces an additional scale associated with the potential valley. We found that its residual imprint persists even in the single-peaked regime, producing a spectrally unstable off-peak family, while the peak modes localized near the potential maximum remain much more spectrally stable.

We then extracted QNMs from time-domain signals for $l = 10$ and $l = 2$. In the $l = 10$, the waveform remains dominated by the spectrally stable peak modes even when the fundamental QNM is overtaken by the off-peak family, whose contribution is negligible. For $l = 2$, the smaller spectral-stability gap enhances the off-peak contribution, allowing the $n_o = 0$ off-peak mode to be recovered at late times.

Our results show that, when distinct QNM families coexist, the spectrally more stable family can dominate the ringdown waveform, while the less stable family remains subdominant, with its suppression increasing with the stability gap. This provides a concrete time-domain link between spectral stability and observational dominance, supporting the robustness of black hole spectroscopy.

Acknowledgments. We are grateful to Yiqian Chen and Lang Cheng for useful discussions and valuable comments. This work is supported in part by NSFC (Grants No. 12275183 and No. 12275184).

Data availability. The data that support the findings of this article are not publicly available upon publication because it is not technically feasible and/or the cost of preparing, depositing, and hosting the data would be prohibitive within the terms of this research project. The data are available from the authors upon reasonable request.

[1] B. P. Abbott *et al.*, Observation of gravitational waves from a binary black hole merger, Phys. Rev. Lett. **116**, 061102 (2016).
[2] B. P. Abbott *et al.*, GW170817: Observation of gravitational waves from a binary neutron star inspiral, Phys. Rev. Lett. **119**, 161101 (2017).
[3] B. P. Abbott *et al.*, Tests of general relativity with GW170817, Phys. Rev. Lett. **123**, 011102 (2019).
[4] R. Abbott *et al.*, Tests of general relativity with binary black holes from the second LIGO-Virgo gravitational-wave transient catalog, Phys. Rev. D **103**, 122002 (2021).
[5] A. G. Abac *et al.*, GWTC-4.0: An introduction to Version 4.0 of the gravitational-wave transient catalog, Astrophys. J. Lett. **995**, L18 (2025).
[6] C. V. Vishveshwara, Stability of the Schwarzschild metric, Phys. Rev. D **1**, 2870 (1970).
[7] Saul A. Teukolsky, Perturbations of a rotating black hole. 1. Fundamental equations for gravitational electromagnetic and neutrino field perturbations, Astrophys. J. **185**, 635 (1973).
[8] S. Chandrasekhar and Steven L. Detweiler, The quasinormal modes of the Schwarzschild black hole, Proc. R. Soc. A **344**, 441 (1975).
[9] E. W. Leaver, An Analytic representation for the quasi normal modes of Kerr black holes, Proc. R. Soc. A **402**, 285 (1985).
[10] S. Chandrasekhar, *The Mathematical Theory of Black Holes* (Clarendon Press, Oxford, 1983).
[11] Edward W. Leaver, Spectral decomposition of the perturbation response of the Schwarzschild geometry, Phys. Rev. D **34**, 384 (1986).
[12] Kostas D. Kokkotas and Bernd G. Schmidt, Quasinormal modes of stars and black holes, Living Rev. Relativity **2**, 2 (1999).
[13] Hans-Peter Nollert, TOPICAL REVIEW: Quasinormal modes: The characteristic 'sound' of black holes and neutron stars, Classical Quantum Gravity **16**, R159 (1999).
[14] Olaf Dreyer, Bernard J. Kelly, Badri Krishnan, Lee Samuel Finn, David Garrison, and Ramon Lopez-Aleman, Black hole spectroscopy: Testing general relativity through gravitational wave observations, Classical Quantum Gravity **21**, 787 (2004).
[15] Emanuele Berti, Vitor Cardoso, and Andrei O. Starinets, Quasinormal modes of black holes and black branes, Classical Quantum Gravity **26**, 163001 (2009).
[16] R. A. Konoplya and A. Zhidenko, Quasinormal modes of black holes: From astrophysics to string theory, Rev. Mod. Phys. **83**, 793 (2011).
[17] Vishal Baibhav, Emanuele Berti, Vitor Cardoso, and Gaurav Khanna, Black hole spectroscopy: Systematic errors and ringdown energy estimates, Phys. Rev. D **97**, 044048 (2018).
[18] Emanuele Berti *et al.*, Black hole spectroscopy: From theory to experiment, arXiv:2505.23895.
[19] B. Carter, Axisymmetric black hole has only two degrees of freedom, Phys. Rev. Lett. **26**, 331 (1971).
[20] D. C. Robinson, Uniqueness of the Kerr black hole, Phys. Rev. Lett. **34**, 905 (1975).
[21] B. P. Abbott *et al.*, Tests of general relativity with GW150914, Phys. Rev. Lett. **116**, 221101 (2016); **121**, 129902(E) (2018).
[22] Richard H. Price and Gaurav Khanna, Gravitational wave sources: Reflections and echoes, Classical Quantum Gravity **34**, 225005 (2017).
[23] Gregorio Carullo, Walter Del Pozzo, and John Veitch, Observational black hole spectroscopy: A time-domain multimode analysis of GW150914, Phys. Rev. D **99**, 123029 (2019); **100**, 089903(E) (2019).
[24] Matthew Giesler, Maximiliano Isi, Mark A. Scheel, and Saul Teukolsky, Black hole ringdown: The importance of overtones, Phys. Rev. X **9**, 041060 (2019).
[25] Vitor Cardoso and Paolo Pani, Testing the nature of dark compact objects: A status report, Living Rev. Relativity **22**, 4 (2019).
[26] Swetha Bhagwat, Xisco Jimenez Forteza, Paolo Pani, and Valeria Ferrari, Ringdown overtones, black hole spectros-

copy, and no-hair theorem tests, Phys. Rev. D **101**, 044033 (2020).
[27] Juan Calderón Bustillo, Paul D. Lasky, and Eric Thrane, Black-hole spectroscopy, the no-hair theorem, and GW150914: Kerr versus Occam, Phys. Rev. D **103**, 024041 (2021).
[28] Maximiliano Isi and Will M. Farr, Analyzing black-hole ringdowns, arXiv:2107.05609.
[29] Collin D. Capano, Miriam Cabero, Julian Westerweck, Jahed Abedi, Shilpa Kastha, Alexander H. Nitz, Yi-Fan Wang, Alex B. Nielsen, and Badri Krishnan, Multimode quasinormal spectrum from a perturbed black hole, Phys. Rev. Lett. **131**, 221402 (2023).
[30] Sizheng Ma, Ling Sun, and Yanbei Chen, Black hole spectroscopy by mode cleaning, Phys. Rev. Lett. **130**, 141401 (2023).
[31] Vishal Baibhav, Mark Ho-Yeuk Cheung, Emanuele Berti, Vitor Cardoso, Gregorio Carullo, Roberto Cotesta, Walter Del Pozzo, and Francisco Duque, Agnostic black hole spectroscopy: Quasinormal mode content of numerical relativity waveforms and limits of validity of linear perturbation theory, Phys. Rev. D **108**, 104020 (2023).
[32] The LIGO Scientific, the Virgo, and the KAGRA Collaborations, Black hole spectroscopy and tests of general relativity with GW250114, Phys. Rev. Lett. **136**, 041403 (2026).
[33] Mark Ho-Yeuk Cheung, Kyriakos Destounis, Rodrigo Panosso Macedo, Emanuele Berti, and Vitor Cardoso, Destabilizing the fundamental mode of black holes: The Elephant and the Flea, Phys. Rev. Lett. **128**, 111103 (2022).
[34] Aubin Courty, Kyriakos Destounis, and Paolo Pani, Spectral instability of quasinormal modes and strong cosmic censorship, Phys. Rev. D **108**, 104027 (2023).
[35] Vitor Cardoso, Shilpa Kastha, and Rodrigo Panosso Macedo, Physical significance of the black hole quasinormal mode spectra instability, Phys. Rev. D **110**, 024016 (2024).
[36] A. Ianniccari, A. J. Iovino, A. Kehagias, P. Pani, G. Perna, D. Perrone, and A. Riotto, Deciphering the instability of the black hole ringdown quasinormal spectrum, Phys. Rev. Lett. **133**, 211401 (2024).
[37] Yiqiu Yang, Zhan-Feng Mai, Run-Qiu Yang, Lijing Shao, and Emanuele Berti, Spectral instability of black holes: Relating the frequency domain to the time domain, Phys. Rev. D **110**, 084018 (2024).
[38] Valentin Boyanov, On destabilising quasi-normal modes with a radially concentrated perturbation, Front. Phys. **12**, 1511757 (2024).
[39] Andrew Laeuger, Colin Weller, Dongjun Li, and Yanbei Chen, The ringdown of a black hole surrounded by a thin shell of matter, Phys. Rev. D **112**, 084042 (2025).
[40] Shui-Fa Shen, Guan-Ru Li, Ramin G. Daghigh, Jodin C. Morey, Michael D. Green, Wei-Liang Qian, and Rui-Hong Yue, Asymptotic quasinormal modes, echoes, and black hole spectral instability: A brief review, Int. J. Mod. Phys. D **35**, 2630001 (2026).
[41] Zhan-Feng Mai and Run-Qiu Yang, Butterfly in spacetime: Inherent instabilities in stable black holes, arXiv:2506.07562.
[42] Mateus Malato Corrêa, Caio F. B. Macedo, Rodrigo Panosso Macedo, and Leandro A. Oliveira, Black hole spectral instabilities in the laboratory: Shallow water analog, Phys. Rev. D **112**, 024036 (2025).
[43] Liang-Bi Wu, Libo Xie, Yu-Sen Zhou, Zong-Kuan Guo, and Rong-Gen Cai, Waveform stability for the piecewise step approximation of Regge-Wheeler potential, Eur. Phys. J. C **86**, 387 (2026).
[44] José Luis Jaramillo, Rodrigo Panosso Macedo, and Lamis Al Sheikh, Pseudospectrum and black hole quasinormal mode instability, Phys. Rev. X **11**, 031003 (2021).
[45] Kyriakos Destounis, Rodrigo Panosso Macedo, Emanuele Berti, Vitor Cardoso, and José Luis Jaramillo, Pseudospectrum of Reissner-Nordström black holes: Quasinormal mode instability and universality, Phys. Rev. D **104**, 084091 (2021).
[46] José Luis Jaramillo, Rodrigo Panosso Macedo, and Lamis Al Sheikh, Gravitational wave signatures of black hole quasinormal mode instability, Phys. Rev. Lett. **128**, 211102 (2022).
[47] José Luis Jaramillo, Pseudospectrum and binary black hole merger transients, Classical Quantum Gravity **39**, 217002 (2022).
[48] Subhodeep Sarkar, Mostafizur Rahman, and Sumanta Chakraborty, Perturbing the perturbed: Stability of quasinormal modes in presence of a positive cosmological constant, Phys. Rev. D **108**, 104002 (2023).
[49] Daniel Areán, David García Fariña, and Karl Landsteiner, Pseudospectra of holographic quasinormal modes, J. High Energy Phys. 12 (2023) 187.
[50] Li-Ming Cao, Jia-Ning Chen, Liang-Bi Wu, Libo Xie, and Yu-Sen Zhou, The pseudospectrum and spectrum (in)stability of quantum corrected Schwarzschild black hole, Sci. China Phys. Mech. Astron. **67**, 100412 (2024).
[51] Jia-Ning Chen, Liang-Bi Wu, and Zong-Kuan Guo, The pseudospectrum and transient of Kaluza–Klein black holes in Einstein–Gauss–Bonnet gravity, Classical Quantum Gravity **41**, 235015 (2024).
[52] Shu Luo, Quasinormal modes, pseudospectrum and time evolution of Proca fields in a quantum Oppenheimer-Snyder–de Sitter spacetime, Phys. Rev. D **110**, 084071 (2024).
[53] Li-Ming Cao, Liang-Bi Wu, and Yu-Sen Zhou, The (in) stability of quasinormal modes of Boulware-Deser-Wheeler black hole in the hyperboloidal framework, Sci. China Phys. Mech. Astron. **68**, 100411 (2025).
[54] Pedro Henrique Croti Siqueira, Lucas Tobias de Paula, Rodrigo Panosso Macedo, and Maurício Richartz, Probing the unstable spectrum of Schwarzschild-like black holes, Phys. Rev. D **111**, 104039 (2025).
[55] Rong-Gen Cai, Li-Ming Cao, Jia-Ning Chen, Zong-Kuan Guo, Liang-Bi Wu, and Yu-Sen Zhou, Pseudospectrum for the Kerr black hole with spin $s = 0$ case, Phys. Rev. D **111**, 084011 (2025).
[56] Li-Ming Cao, Ming-Fei Ji, Liang-Bi Wu, and Yu-Sen Zhou, Pseudospectrum and time-domain analysis of the EFT corrected black holes, Phys. Rev. D **112**, 124022 (2025).

[57] Enrico Barausse, Vitor Cardoso, and Paolo Pani, Can environmental effects spoil precision gravitational-wave astrophysics?, Phys. Rev. D **89**, 104059 (2014).

[58] Emanuele Berti, Vitor Cardoso, Mark Ho-Yeuk Cheung, Francesco Di Filippo, Francisco Duque, Paul Martens, and Shinji Mukohyama, Stability of the fundamental quasinormal mode in time-domain observations against small perturbations, Phys. Rev. D **106**, 084011 (2022).

[59] Thomas F. M. Spieksma, Vitor Cardoso, Gregorio Carullo, Matteo Della Rocca, and Francisco Duque, Black hole spectroscopy in environments: Detectability prospects, Phys. Rev. Lett. **134**, 081402 (2025).

[60] Naritaka Oshita, Emanuele Berti, and Vitor Cardoso, Unstable chords and destructive resonant excitation of black hole quasinormal modes, Phys. Rev. Lett. **135**, 031401 (2025).

[61] Koutarou Kyutoku, Hayato Motohashi, and Takahiro Tanaka, Quasinormal modes of Schwarzschild black holes on the real axis, Phys. Rev. D **107**, 044012 (2023).

[62] Sizheng Ma, Keefe Mitman, Ling Sun, Nils Deppe, François Hébert, Lawrence E. Kidder, Jordan Moxon, William Throwe, Nils L. Vu, and Yanbei Chen, Quasinormal-mode filters: A new approach to analyze the gravitational-wave ringdown of binary black-hole mergers, Phys. Rev. D **106**, 084036 (2022).

[63] Naritaka Oshita, Greybody factors imprinted on black hole ringdowns: An alternative to superposed quasinormal modes, Phys. Rev. D **109**, 104028 (2024).

[64] Theo Torres, From black hole spectral instability to stable observables, Phys. Rev. Lett. **131**, 111401 (2023).

[65] Wen-Di Guo, Qin Tan, and Yu-Xiao Liu, Quasinormal modes and greybody factor of a Lorentz-violating black hole, J. Cosmol. Astropart. Phys. 07 (2024) 008.

[66] Kazumasa Okabayashi and Naritaka Oshita, Greybody factors imprinted on black hole ringdowns. II. Merging binary black holes, Phys. Rev. D **110**, 064086 (2024).

[67] Romeo Felice Rosato, Kyriakos Destounis, and Paolo Pani, Ringdown stability: Graybody factors as stable gravitational-wave observables, Phys. Rev. D **110**, L121501 (2024).

[68] Naritaka Oshita, Kazufumi Takahashi, and Shinji Mukohyama, Stability and instability of the black hole greybody factors and ringdowns against a small-bump correction, Phys. Rev. D **110**, 084070 (2024).

[69] Guan-Ru Li, Wei-Liang Qian, Qiyuan Pan, Ramin G. Daghigh, Jodin C. Morey, and Rui-Hong Yue, Regge poles, greybody factors, and absorption cross sections for black hole metrics with discontinuity, Phys. Rev. D **112**, 064071 (2025).

[70] Libo Xie, Liang-Bi Wu, and Zong-Kuan Guo, Spectrum instability and graybody factor stability for parabolic approximation of Regge-Wheeler potential, Phys. Rev. D **112**, 024054 (2025).

[71] Carlos A. R. Herdeiro, Eugen Radu, Nicolas Sanchis-Gual, and José A. Font, Spontaneous scalarization of charged black holes, Phys. Rev. Lett. **121**, 101102 (2018).

[72] Qingyu Gan, Peng Wang, Houwen Wu, and Haitang Yang, Photon ring and observational appearance of a hairy black hole, Phys. Rev. D **104**, 044049 (2021).

[73] Cheng-Yong Zhang, Qian Chen, Yunqi Liu, Wen-Kun Luo, Yu Tian, and Bin Wang, Critical phenomena in dynamical scalarization of charged black holes, Phys. Rev. Lett. **128**, 161105 (2022).

[74] Guangzhou Guo, Peng Wang, and Yupeng Zhang, Nonlinear stability of black holes with a stable light ring, Phys. Rev. D **112**, 084023 (2025).

[75] Guangzhou Guo, Peng Wang, Houwen Wu, and Haitang Yang, Scalarized Kerr-Newman black holes, J. High Energy Phys. 10 (2023) 076.

[76] See Supplemental Material at http://link.aps.org/supplemental/10.1103/srxw-wsvq for details on spectral methods, migration rates, waveform evolution, and fitting procedures.

[77] J. P. Boyd, *Chebyshev and Fourier Spectral Methods* (Courier Corporation, Mineola, NY, 2001).

[78] Anil Zenginoglu, Hyperboloidal foliations and scri-fixing, Classical Quantum Gravity **25**, 145002 (2008).

[79] Anil Zenginoglu, A geometric framework for black hole perturbations, Phys. Rev. D **83**, 127502 (2011).

[80] Rodrigo Panosso Macedo, Hyperboloidal approach for static spherically symmetric spacetimes: A didactical introductionand applications in black-hole physics, Phil. Trans. R. Soc. A **382**, 20230046 (2024).

[81] Aron Jansen, Overdamped modes in Schwarzschild-de Sitter and a Mathematica package for the numerical computation of quasinormal modes, Eur. Phys. J. Plus **132**, 546 (2017).

[82] Zhiying Zhu, Shao-Jun Zhang, C. E. Pellicer, Bin Wang, and Elcio Abdalla, Stability of Reissner-Nordström black hole in de Sitter background under charged scalar perturbation, Phys. Rev. D **90**, 044042 (2014); **90**, 049904(A) (2014).

[83] Yang Huang and Dao-Jun Liu, Charged scalar perturbations around a regular magnetic black hole, Phys. Rev. D **93**, 104011 (2016).

[84] R. A. Konoplya and A. Zhidenko, Massive charged scalar field in the Kerr-Newman background I: Quasinormal modes, late-time tails and stability, Phys. Rev. D **88**, 024054 (2013).

[85] Vitor Cardoso, Alex S. Miranda, Emanuele Berti, Helvi Witek, and Vilson T. Zanchi, Geodesic stability, Lyapunov exponents and quasinormal modes, Phys. Rev. D **79**, 064016 (2009).

[86] Minyong Guo, Zhen Zhong, Jinguang Wang, and Sijie Gao, Light rings and long-lived modes in quasiblack hole spacetimes, Phys. Rev. D **105**, 024049 (2022).

[87] Guangzhou Guo, Peng Wang, Houwen Wu, and Haitang Yang, Quasinormal modes of black holes with multiple photon spheres, J. High Energy Phys. 06 (2022) 060.

[88] Guangzhou Guo, Peng Wang, Houwen Wu, and Haitang Yang, Echoes from hairy black holes, J. High Energy Phys. 06 (2022) 073.

[89] Zhen-Hao Yang, Liang-Bi Wu, Xiao-Mei Kuang, and Wei-Liang Qian, QNM families: Classification and competition, Phys. Rev. D **113**, 044072 (2026).

[90] Kazuto Takahashi and Hayato Motohashi, Iterative extraction of overtones from black hole ringdown, Classical Quantum Gravity **41**, 195023 (2024).